Journal Pre-proof
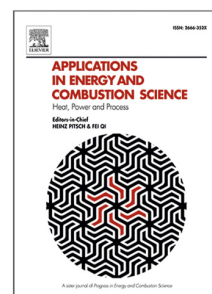
Steady laminar stagnation flow NH$_3$-H$_2$-air flame at a plane wall: Flame extinction limit and its influence on the thermo-mechanical stress and corrosive behavior of wall materials

Chunkan Yu, Surabhi Srikanth, Thomas Böhlke, Bronislava Gorr, Ulrich Maas

Please cite this article as: C. Yu, S. Srikanth, T. Böhlke et al., Steady laminar stagnation flow NH$_3$-H$_2$-air flame at a plane wall: Flame extinction limit and its influence on the thermo-mechanical stress and corrosive behavior of wall materials. *Applications in Energy and Combustion Science* (2024), doi: https://doi.org/10.1016/j.jaecs.2024.100261.

This is a PDF file of an article that has undergone enhancements after acceptance, such as the addition of a cover page and metadata, and formatting for readability, but it is not yet the definitive version of record. This version will undergo additional copyediting, typesetting and review before it is published in its final form, but we are providing this version to give early visibility of the article. Please note that, during the production process, errors may be discovered which could affect the content, and all legal disclaimers that apply to the journal pertain.

Steady laminar stagnation flow NH_3-H_2-air flame at a plane wall: flame extinction limit and its influence on the thermo-mechanical stress and corrosive behavior of wall materials

Chunkan Yu[a], Surabhi Srikanth[a], Thomas Böhlke[b], Bronislava Gorr[c], Ulrich Maas[a]

[a]*Institute of Technical Thermodynamics (ITT), Karlsruhe Institute of Technology (KIT), Engelbert-Arnold-Str. 4, Karlsruhe, 76131, Baden Württemberg, Germany*
[b]*Institute of Engineering Mechanics, Chair for Continuum Mechanics, Karlsruhe Institute of Technology (KIT), Kaiserstrasse 10, Karlsruhe, 76131, Baden Württemberg, Germany*
[c]*Institute for Applied Materials - Applied Materials Physics (IAM-AMP), Karlsruhe Institute of Technology (KIT), Hermann-von Helmholtz-Platz 1, Karlsruhe, 76344, Baden Württemberg, Germany*

Abstract

The steady laminar stagnation flow flame of NH_3-H_2-air gas mixture stabilized at a plane wall is numerically investigated. Its interaction with the wall with the consideration of heat loss is the focus of this work. The numerical study of the combustion system is performed by using the full chemical mechanism and detailed transport model including the differential diffusion and Soret effect. The simulation of the solid mechanics is based on the theory of isotropic linear thermo-elasticity. With the numerical simulation, it will be discussed how the wall material would change the flame stability in terms of extinction limit, and how the combustion system such as mixture composition, flame strain rate, and pressure would vary the thermo-mechanical stresses in the solid wall and the corrosive behavior at the surface of the wall.

Keywords:
ammonia, hydrogen enrichment, stagnation flow flame, thermo-mechanical stress, corrosion

1. Introduction

In most of the combustion applications such as gas turbines and furnaces, the combustion process closely interacts with the solid material. Flame-solid interaction refers to the complex and dynamic interactions that occur between flames and solid materials. This interaction plays a crucial role in a wide range of processes, including the combustion of gaseous or solid fuels, flame spread, and material mechanics. On one hand, the selection of materials can significantly affect the combustion efficiency and combustion properties such as combustion temperature and NOx emission [1, 2, 3]. For example, as reported in [2], if the combustion chamber head is made from aluminum alloy, it could cause a higher HC formation compared to cast iron, and the coating of the surface with low heat conductivity improves the combustion efficiency. On the other hand, the combustion process could also have a noticeable influence on the material and mechanical properties such as thermal stress and creep lifetime. For instance, in [4] it is shown that the optimization of the combustion process is re-

quired to avoid thermal failure on a combustion liner, and in [5] it is stated that the thermoacoustic instability leads to different wall displacement of the combustion chamber.

Despite several existing literatures about the flame-solid interaction, there is still limited study concerning the numerical modeling of this interaction, and the interaction of materials with clean fuels (low and zero carbon fuels) is still desired. There is a pressing need to develop clean fuel technologies to offset the undesirable effects of climate change and combat the depletion of conventional fuels. Ammonia's widespread availability, comparatively low Nox emissions, and high volumetric density make it an attractive material for clean fuel. However, the use of ammonia has several severe application problems. For example, ammonia can be corrosive to various metals (e.g. copper and brass), so containers made from these metals to store the ammonia gas must be avoided [6, 7]. Furthermore, the ammonia-hydrogen system leads to hydrogen embrittlement and induces stress corrosion cracking. [8, 9].

Hence, with the increasing demand for the use of ammonia in different applications such as furnaces, internal combustion engines, gas turbines, and fuel cells, it is also important to investigate how the ammonia combustion system behaves if it interacts with solid materials in terms of thermo-mechanical stresses, corrosive layer growth at the surface, etc.

This paper analyses the steady laminar stagnation flow of NH3-H2-air flame at a plane wall with a focus on the extinction limit and the influence of combustion system on the thermo-mechanical stress and corrosive behaviors. Though there are various studies about the mechanical and combustion properties of gas and solid considered as individual systems, there is still a gap in understanding the exact coupling behavior between the flame and the wall. It should be emphasized that the applied models are not only restricted to the ammonia system but are also relevant for all other combustion processes in real applications. And this understanding can help improve the efficiency of the combustion process and reduce the damage to the wall surface.

2. Mathematical Modeling

In the present work, study of the flame-solid interaction focuses on the combustion configuration of the stagnation flow premixed flames to a plane wall, as shown in Fig.1. In this configuration, fuel and oxidizer are pre-mixed and flow out of the burner nozzle, and a flame (gas phase) impinging normal to a plane surface is observed.
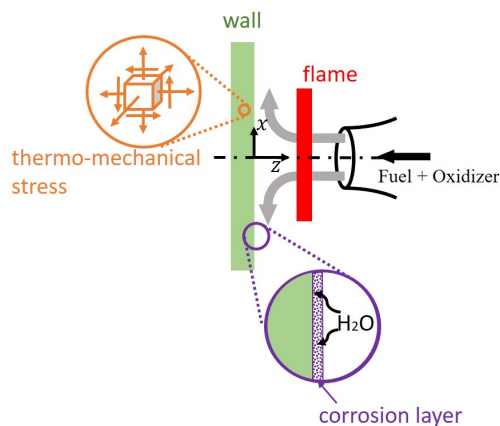

Figure 1: Schematical illustration of the stagnation flow premixed flame to a plane wall.

Due to the high temperature of premixed flames, the temperature inside the plane wall (solid phase) is not homogeneously distributed, inducing thermo-mechanical stress caused by the temperature change in the material (orange part in Fig.1).

Moreover, because of the high temperature at the contact surface ($z = 0$ mm) and the presence of oxygen (dissociated from water vapor as a major product) and other molecular sources from the exhaust gas, the wall material can experience significant changes as a result of high-temperature corrosion. In particular, depending on the chemical composition of the wall material, constitution of the exhaust gas, and temperature, an oxide layer will continuously grow on the metallic wall (purple part in Fig.1). Due to the addition of specific elements such as Cr, Al or Si in a proper concentration, the surface of the alloy will be completely covered by Cr_2O_3, Al_2O_3 or SiO_2 layer. Such protective oxide scales separate the metallic substrate from the gas phase preventing oxidation of the main element, i.e, Ni in Ni-based alloys (e.g, stainless steel), and therefore fast degradation of the materials such as nitriding [10, 11].

2.1. Governing equations in the gas phase of a stagnation flow flame ($z > 0$)

In general, the numerical simulation for the considered flame configuration can be performed in a two-dimensional (2D) or even three-dimensional (3D) geometry. However, a study in [12] shows that although the 1D simulation results tend to over-predict the velocity field, the 1D simulation can give accurate predictions for the temperature field of the flame. As already shown in various publications such as [13, 14, 15], the 1D simulation can give an accurate prediction for the flame structure and the flame extinction limit against the experimental measurements if several assumptions and simplifications are made. Furthermore, in the pratical application, the Reynolds number increases with increasing pressure and the flow tends to transit to turbulence. However, since we want to keep the problem as simple as possible to avoid the influence of turbulence with the corresponding turbulence models in the discussion, we assume that the flow remains laminar for the whole pressure range ($p < 20$ bar for this study).

In the present, we follow the modeling in [16, 17], and the following assumptions and simplifications are made for the flame (gas phase):

- The ideal gas law is valid for the whole combustion pressure condition ($p \leq 20$ bar) considered in the present work.

- The isobaric laminar premixed flame normally impinging onto a plane wall is considered in the present, and the flow in the burner is assumed to be an axisymmetric stagnation flow. This means that all thermo-kinetic quantities (e.g. temperature, species mass fractions) of the flame along the symmetric line can be solved for functions of the z coordinate.

- Thermal radiation is neglected in flame modeling. However, it should be noted that the consideration of thermal radiation may increase additional thermal load inside the solid, which is a subject of future research.

- All thermo-physical properties are isotropic and temperature-dependent: they involve density ρ_g, isobaric specific heat capacity $c_{p,g}$, dynamic viscosity η_g, heat conductivity k_g and molecular diffusion coefficients $D_{i,g}$ of species i. Here the subscript $_g$ represents the quantities for flame in gas phase.

Although the flow field is two-dimensional, according to Refs.[16, 17], all the governing equations can be re-formulated as a set of partial differential equations depending only on z-coordinate (c.f. Fig.1) by introducing two independent parameters: the tangential pressure gradient J and the tangential velocity gradient G:

$$G(z,t) = \frac{v_x(z,t)}{x}, \tag{1}$$

$$J = -\frac{1}{x}\frac{\partial p_g}{\partial x}, \tag{2}$$

where v_x is the flow velocity in radial direction (c.f. Fig.1), and p_g is the pressure of the gas mixture. Conse-

quently, the following set of equations is obtained [16]:

$$\frac{\partial \rho_g}{\partial t} = -2\rho_g G - \frac{\partial (\rho_g v_z)}{\partial z}, \tag{3}$$

$$\frac{\partial G}{\partial t} = -\frac{J}{\rho_g} - G^2 + \frac{1}{\rho_g}\frac{\partial}{\partial z}\left(\eta_g \frac{\partial G}{\partial z}\right) - v_z\frac{\partial G}{\partial z}, \tag{4}$$

$$\frac{\partial v_z}{\partial t} = -\frac{4}{3\rho_g}\frac{\partial}{\partial z}(\eta_g G) + \frac{2\eta_g}{\rho_g}\frac{\partial G}{\partial z}$$
$$+ \frac{4}{3\rho_g}\frac{\partial}{\partial z}\left(\eta_g \frac{\partial v_z}{\partial z}\right) - v_z\frac{\partial v_z}{\partial z}, \tag{5}$$

$$\frac{\partial T_g}{\partial t} = -\frac{1}{\rho_g c_{p,g}}\frac{\partial j_{q,g}}{\partial z} - \frac{1}{\rho_g c_{p,g}}\sum_{i=1}^{n_s}\dot{\omega}_i \bar{h}_i$$
$$- v_z\frac{\partial T_g}{\partial z}, \tag{6}$$

$$\frac{\partial w_i}{\partial t} = -\frac{1}{\rho_g}\frac{\partial j_{i,g}}{\partial z} + \frac{\dot{\omega}_i M_i}{\rho_g} - v_z\frac{\partial w_i}{\partial z}, \tag{7}$$

$$0 = \rho_g - \frac{p_g \bar{M}}{R T_g}. \tag{8}$$

In these equations, n_s denotes the number of species involved in the chemical reactions. T_g is the temperature of the gas mixture. v_z is the flow velocity in axial direction. For species i, it has the mass fraction w_i, molar mass M_i, molar enthalpies $\bar{h}_i$, molar rates of formation due to chemical reaction $\dot{\omega}_i$ (see Refs.[18] for details). The energy transport flux $j_{q,g}$ is determined as

$$j_{q,g} = -k_g\frac{\partial T_g}{\partial z} + T_g\sum_{i=1}^{n_s}c_{pi}j_{i,g}, \tag{9}$$

and molecular diffusion fluxes $j_{i,g}$ are calculated as

$$j_{i,g} = -\rho_g D_{i,g}^D\frac{w_i}{x_i}\frac{\partial x_i}{\partial z} - \frac{D_{i,g}^T}{T_g}\frac{\partial T_g}{\partial z}. \tag{10}$$

Here x_i is the mole fraction of i−th species. D_i^D represents the mass diffusion coefficient, and D_i^T is the thermal diffusion coefficient for the Soret effect. Both $D_{i,g}^D$ and $D_{i,g}^T$ are calculated according to Ref.[19].

Note that here the Dufour effect (energy transport due to species concentration gradient) and the pressure diffusion (diffusion caused by pressure gradient) are not considered in the numerical simulation, because their effects are negligibly small in combustion systems [20, 21].

2.2. Governing equations in the solid phase of a plane wall ($z < 0$)

Metallic components loaded under the generally temperature-dependent yield or damage stress behave

3

thermoelastically. This thermoelastic behavior can be described with a linear thermoelastic theory for small deformations. The material coefficients are the elastic stiffness and the thermal expansion coefficients [22, 23, 24]. Alternatively, compliance and thermal stresses can be used. The stiffnesses and compliances are fourth-order tensors with generally twenty-one constants, and the thermal expansion coefficients and temperature stresses are second-order tensors with six constants [24, 25]. In the isotropic case, the numbers reduce from twenty-one to two and from six to one. In general, these coefficients can be strongly temperature dependent. Consideration of mechanically and thermally induced stresses is important because both can be of the same magnitude and therefore must be taken into account when dimensioning engineering components. If the yield stress is reached, inelastic deformations may occur and thermoelastic modeling must be used by thermoelastoplastic modeling, e.g. with a temperature-dependent variant of the von Mises plasticity model [26].

In this work, we restrict ourselves to the most simple case for the plane wall in solid phase, in which the following assumptions and simplifications are made:

- The strain is small such that the theory of geometrically and physically linear thermoelasticity is valid, and the thermoelastic behavior is assumed to be isotropic.

- The elastic parameters are temperature dependent. These properties involve mass density ρ_s, isochoric specific heat capacity $c_{v,s}$, heat conductivity k_s, coefficient of thermal expansion α_s, Young's modulus E_s, shearing modulus G_s.

- The temperature inside the plane wall depends only on $z-$coordinate.

- The displacement field is only dependent on the $z-$coordinate and the displacement in $x-$ and $y-$directions disappear ($u_x = u_y = 0$). This means that in this coordinate system only the normal stresses exist ($\sigma_{xy} = \sigma_{xz} = \sigma_{yz} = 0$), and the corresponding thermo-mechanical stress in the plane wall is reduced to

$$\underline{\underline{\sigma}} = \begin{pmatrix} \sigma_{xx} & 0 & 0 \\ 0 & \sigma_{yy} & 0 \\ 0 & 0 & \sigma_{zz} \end{pmatrix}. \tag{11}$$

Based on these simplifications and assumptions, the equation for heat conduction in spatial one-dimensional

coordinate reads [24, 27]

$$\rho_s c_{v,s} \frac{\partial T_s}{\partial t} = \frac{\partial}{\partial z}\left(k_s \frac{\partial T_s}{\partial z}\right) - T_s(3\lambda_s + 2\mu_s)\alpha_s \frac{\partial}{\partial z}\left(\frac{\partial u_z}{\partial t}\right). \tag{12}$$

Note that the second term on the right-hand side of the Eq.12 describes the Gough-Joule effect, which is important e.g. for the transient process with large deformations inducing structural heating [28]. This effect becomes less important if no sudden temperature change occurs and can be neglected only if the steady state of the system is of interest.

The displacement in $z-$direction (u_z) can be calculated through the equation of motion with the absence of body forces as

$$\rho_s \frac{\partial^2 u_z}{\partial t^2} = \frac{\partial}{\partial z}\left[(\lambda_s + 2\mu_s)\frac{\partial u_z}{\partial z}\right] - \frac{\partial}{\partial z}\left[(3\lambda_s + 2\mu_s)\int_{T_0}^{T}\alpha_s(T')dT'\right]. \tag{13}$$

In these equations, λ_s and μ_s denote Lame's constants which are related to E_s and G_s by [24]

$$\lambda_s = \frac{v_s E_s}{(1 + v_s)(1 - 2v_s)}, \tag{14}$$

$$\mu_s = G_s = \frac{E_s}{2(1 + v_s)}, \tag{15}$$

where v_s refers to the Poisson's ratio. Based on the displacement u_z, the corresponding mechanical stresses in the plane wall are formulated as

$$\sigma_{xx} = \sigma_{yy} = \lambda_s \frac{\partial u_z}{\partial z} - (3\lambda_s + 2\mu_s)\int_{T_0}^{T}\alpha_s(T')dT', \tag{16}$$

$$\sigma_{zz} = (\lambda_s + 2\mu_s)\frac{\partial u_z}{\partial z} - (3\lambda_s + 2\mu_s)\int_{T_0}^{T}\alpha_s(T')dT'. \tag{17}$$

Under multi-axial loading conditions, the von Mises equivalent stress σ_{vM} is an important and useful indicator for plastic yielding [29, 30, 31]: if it is less than the tensile yield strength, the material undergoes an elastic deformation; if the yield strength is reached, then the material could undergo a possible plastic deformation if the loading condition is satisfied. For the thermomechanical stresses (c.f. Eq.11), the corresponding von Mises equivalent stress σ_{vM} can be calculated as [31]

$$\sigma_{vM} = \sqrt{\frac{(\sigma_{xx} - \sigma_{yy})^2 + (\sigma_{xx} - \sigma_{zz})^2 + (\sigma_{yy} - \sigma_{zz})^2}{2}} \tag{18}$$

4

Note that in the current thermoelastic modeling for the plane wall, the oxide layer has not been included. To account for the thermo-mechanical stress inside the oxide layer, which is coupled with the plane wall, additional thermoelastic properties (e.g., Young's modulus, shear modulus, coefficient of thermal expansion) must be taken determined and taken into account. This means that in an isotropic case, three additional temperature-dependent material constants need to be a-priori known, which are not easy to determine. This will be included in our future research.

2.3. Corrosion behaviors at the surface ($z = 0$)

At the surface ($z = 0$) oxygen or steam can react with the metallic wall forming an oxide scale that grows with time [32]. It was found that a parabolic rate law can be applied to describe the growth of the oxide layer, and the corresponding growth rate of the corrosion layer can be described by a parabolic oxidation constant k_p, which is usually determined using values of specific mass change as a function of time [33, 10, 11, 34]. And this parabolic oxidation constant has been used for various environmental cases such as oxygen environment or steam environment, whose review reports can be found in e.g. [35, 36] for detailed review.

The parabolic oxidation constant depends mainly on the temperature according to the Arrhenius relation

$$k_p = k_p^0 \exp\left(-\frac{Q}{RT}\right), \tag{19}$$

indicating that the oxidation rate constant k_p increases exponentially with temperature. While the temperature dependence of k_p is straightforward, the dependence of k_p on the gaseous partial pressures is more complicated. This is because the oxygen participating in the building of a corrosive layer can come from different sources such as dissociation of the water molecules or other reactive species such as OH and CO. And different species or their corresponding partial pressures have different effect on the k_p values:

- The dependence of oxygen partial pressure $p(O_2)$ is determined by the defect structure and the dissociated pressure of the oxide as

$$k_p \sim p(O_2)^{\frac{1}{n}}, \tag{20}$$

where the value n is a function of the defect structure of the corresponding oxide [37]. While a monotonic increase of k_p with the temperature is observed, the relation between k_p and $p(O_2)$ is more complicated. A non-monotonic change of k_p with $p(O_2)$ is reported in various literature such as [38, 39, 40].

- The same complicated dependence behavior is also observed in steam environment with varying steam partial pressure $p(H_2O)$. For example, a parabolic dependence between k_p and steam partial pressure has been observed as $k_p \sim p(H_2O)^2$ in [41] for SiC material. However, in [42, 43] non-monotonic tendency of k_p against steam partial pressure are reported. Additionally, compared to the oxide layer formation due to oxygen, the dissociation and adsorption of H_2O at the metallic surface are much faster than those of the O_2, as reported in [44, 45].

It should be pointed out there that the mechanism of growth of corrosion layers in complex environments such as the exhaust gas of combustion process is not properly understood, and the modeling of corrosive growth including all relevant species is difficult [32]. Nevertheless there is still no universal method to determine the k_p values depending on the partial pressures of different species. Hence, in the present work, we will focus on discussing about how the partial pressures of O_2 and H_2O change with the combustion systems, which provides the suggestion about which partial pressures or in which order of magnitude of partial pressures are relevant to investigate the corrosion behavior during the combustion process. An accurate prediction of k_p values for different combustion conditions is thus not possible at this stage, which requires further experimental and numerical investigation.

2.4. Interface ($z = 0$)

For the present work, some model simplification have been made to reduce the complexity of the modeling. Firstly, the solid surface is considered chemically inert, so there is no surface reaction considered for the numerical simulation. However, two major points must be addressed for this point:

- metal walls with specific materials can be highly reactive to ammonia decomposition, such as the thermal decomposition of NH_3 on quartz and stainless steel walls [46] or the NH_3 decomposition on Ni surface [47]. Considering ammonia decomposition at the surface could improve the assessment on the effect of wall materials on flame species profiles.

- As will shown later, there exist considerable amounts of reactive radicals such as hydrogen and oxygen radicals near and at the wall. Therefore, the

5

effect of radical quenching can also be considered [48, 49, 50]. For example, the sticking coefficient values against radicals such as OH, O and H at the Inconel surface can be included in the model [50].

However, to assess the potential impact of surface reactions on flame properties, we consider simple surface recombination/destruction of reactive molecules in Section 4.6. The formation rate of species due to surface reactions is described by the surface destruction efficiency and the surface collision number of the involved species, following the implementation in [51].

Furthermore, the plane wall is assumed to be impermeable, so the molecular diffusion flux at the interface is zero:

$$j_{i,g}(z = 0^+) = 0. \quad (21)$$

It should be pointed out that this is a strong assumption since the nitriding process [52, 53] and hydrogen embrittlement [9] can be clearly observed for the ammonia/hydrogen combustion system. Both processes result in changes in material composition and, consequently, alterations in mechanical properties such as Young's modulus and shear modulus. Coupling both processes with the combustion process is of great interest, which is also the focus of our ongoing research.

Note that in the numerical simulation, the growth of the corrosive layer will not be considered, since they are usually very thin even after several thousand hours. For example, the Ni-based alloy 625 forms a 2 μm thick Cr_2O_3 scale after exposure to an Ar-50% H_2O atmosphere for 10000 h at 750°C [54]. The influence of the oxide scales on the combustion system is assumed to be minor. However, the species concentrations and the temperature at the interface will be used for the determination of the corrosion parabolic rate constant k_p.

In addition, the energy transport flux at the interface must be equal from both sides according to thermal equilibrium, which is formulated as

$$k_s \frac{\partial T_s}{\partial z}\Big|_{z=0^-} = k_g \frac{\partial T_g}{\partial z}\Big|_{z=0^+}. \quad (22)$$

Finally, the pressure of the flame flow at the interface is balanced with the stress of the solid, which is expressed as

$$\sigma_{zz}(z = 0^-) = -p_g(z = 0^+). \quad (23)$$

Here p_g represents pressure from gas phase flame and $-p_g$ represents negative normal stress.

2.5. Numerical simulation

The numerical simulation is performed by using the in-house *INSFLA* code [51], which is originally designed for a pure combustion system and has been validated against experimental measurements for various laminar flame configurations such as premixed flame with flame speed and flammability limit [55, 56], non-premixed flame against extinction [57] and flame-wall interaction including complex surface reactions [58]. The code has been extended to include the heat transfer through the plane wall in solid phase (Eq.12) and the solid displacement (Eq.13). Details about the numerical implementation can be found in previous work [59]. For the efficient computational simulation, an automatic adaptive meshing technique [51] has been applied to capture the domain with high scalar gradients, where more grid points are required for accurate resolution.

3. Studied Model System

3.1. Computational domain

In the present work, the thickness of the plane wall is kept at H =10 mm, which is within a typical thickness of a rotor blade in the gas turbine application [60, 61]. The computational domain for the flame side is Ω = 0.15m, which is sufficiently large for all strain rates under all conditions considered in the flame simulation and the flame is not affected by boundary. Note that this large domain does not reduce the resolution of the flame front due to the adaptive grid system [51].

3.2. Gas mixture and Chemical Mechanisms

In the present work, the ammonia-air systems under hydrogen enrichment are considered. The level of H_2 addition in ammonia is described by the mole fraction α of H_2 in the fuel as

$$\alpha H_2 + (1-\alpha)NH_3 + \frac{1}{\Phi}\left(0.75 - \frac{\alpha}{4}\right)(O_2 + \frac{79}{21}N_2). \quad (24)$$

The Li-2019 detailed chemical mechanism [62], which involves 34 species and 252 reactions for the NH_3-H_2-air combustion system after removing all unnecessary species (hydrocarbon species and inert gases), is used for the numerical simulation. This full chemical mechanism has been well validated against experimental measurements such as ignition delay times, flame speed, and extinction strain rates of NH_3-air and/or MH_3-H_2-air mixtures over a wide range of conditions, as shown in Refs. [62, 55]. Since the extinction

6

limit of the considered strained premixed flame stabilized at a plane wall is the focus of the present work, it is also necessary to validate the Li-2019 mechanism for the extinction limit a_E prediction of the laminar strained premixed flame with recently published measurements from [63], as shown in Fig.2. It is clearly observed that the numerically predicted results using this Li-2019 mechanism give good agreement with experimental measurements (uncertainty ±5% reported in [63]).
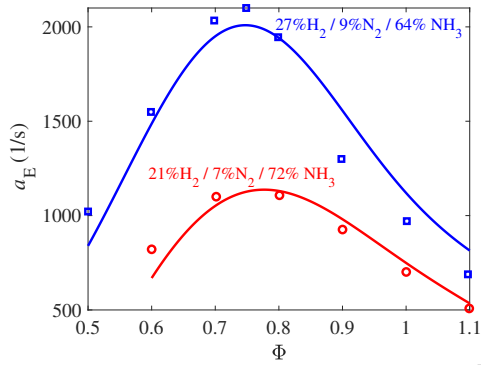

Figure 2: Measured extinction strain rates (symbols) [63] and numerically predicted results using Li-2019 detailed chemical mechanism [62]. Pressure: 1 bar; Unburnt gas temperature: 300 K.

3.3. Material selected for the plane wall

In the present work, Inconel 718 as a nickel-based superalloy is applied for most investigations. Inconel 718 has a number of desirable properties such as high strength, heat resistance, and corrosion resistance. Hence it has a lot of applications in areas subjected to extreme temperatures in aero engines, gas turbines, and cryogenic tankage [64, 65, 66, 67]. Since it is a highly weldable material, it is also largely used in additive manufacturing. The properties of additively manufactured Inconel 718 can have variations, depending on the processes and post-heat treatments used. Electron Beam Melting (EBM) and Selective Laser Melting (SLM) are examples of common processes that are used for additive manufacturing of Inconel 718 [68].

In order to compare the influence of the wall material on the combustion system and of the combustion system on the plane wall, the Ti-6Al-4V as a titanium alloy will also be selected for the wall material to emphasize this issue. Note that although titanium alloy is used for various applications in the aerospace industry due to its high

strength, high corrosion resistance, and fracture toughness, it is only commonly used in "cold" regimes such as low-pressure compressors in gas turbines, and cannot be regarded as a high-temperature material because of its low thermal capability up to 300°C primarily due to its poor oxidation resistance [69]. The selection of Ti-6Al-4V here is only deemed for comparison.

The material properties including heat conductivities, thermal expansion coefficients, Poisson's ratios, and Young's modulus, which are temperature dependent, are listed in Appendix A with corresponding references.

4. Results and Discussion

4.1. Typical temperature and thermo-mechanical stress profiles

Before we begin with the discussion, it is important to give an impression about typical profiles of the temperature (Fig.3), the von Mises stresses σ_{vM} inside the plane wall (Fig.4) and the species mass fractions in the combustion system (Fig.5). For all the simulation shown throughout the whole work, the wall temperature at $z = -10$ mm is set to be a fixed temperature of 300 K which corresponds to the temperature of the unburnt gas mixture: $T(z = -10\text{mm}) = T_{ub} = 300$ K.

It can be observed from Fig.3 that the temperature inside the plane wall increases from the cold side ($z = -10$ mm) to the contact surface ($z = 0$ mm). It should be mentioned that the temperature gradient inside the wall is not constant because of the temperature-dependent heat conductivity, ensuring a constant heat flux inside the wall at steady state. Another straightforward conclusion is that at the contact surface, the temperature gradient inside the wall is much smaller than the one from the combustion system: $\left.\frac{\partial T_s}{\partial z}\right|_{z=0^-} < \left.\frac{\partial T_g}{\partial z}\right|_{z=0^+}$, because the heat conductivity of the solid is usually larger than that of one of the gas mixtures for a wide temperature range: $k_s > k_g$.

Based on the temperature profile inside the plane wall, the corresponding profile of the von Mises stresses σ_{vM} (c.f. Fig.4) shows that σ_{vM} changes monotonically inside the plane wall and reaches its maximum at the contact surface ($z = 0$ mm) where the wall has its maximum temperature. Moreover, in this figure, the yield strength σ_Y based on the temperature profile inside the plane wall is also presented (red solid line). The yield strength is strongly temperature dependent, [70] and Inconel 718 has a high yield strength till around 900 K (around 600°C), which then decreases sharply to approximately 1225 K (around 950°C). In this shown example, σ_{vM} is well below the yield strength, indicat-

7
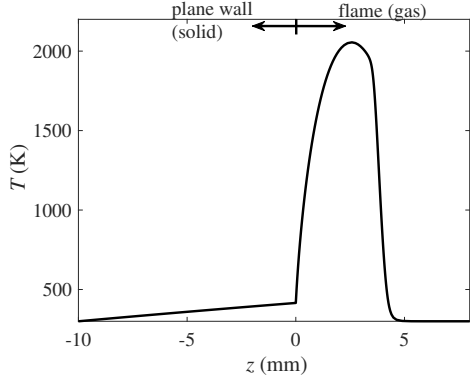
Figure 3: Typical temperature profiles of the flame (gas phase) and inside the plane wall (solid phase). Combustion system: stoichiometric NH_3-H_2-mixture with 40% hydrogen addition under $p = 1$ bar and $T_{ub} = 300$ K. Flame strain rate: $a = 300$ s^{-1}. Material: Inconel 718.

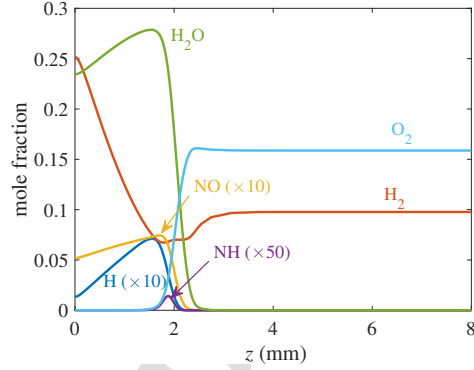ing an elastic formation. Later we will show that under some conditions σ_{vM} would be beyond the yield strength, which causes more complicated material deformation behavior.
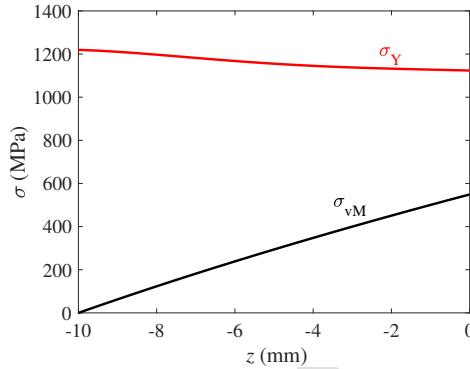

Figure 4: Typical profile of the von Mises stresses σ_{vM} and the yield strength σ_Y inside the plane wall (solid phase). Combustion system: stoichiometric NH_3-H_2-mixture with 40% hydrogen addition under $p = 1$ bar and $T_{ub} = 300$ K. Flame strain rate: $a = 300$ s^{-1}. Material: Inconel 718.

In Fig.5 typical profiles of mole fractions of several major and minor species in the flame are presented. We should emphasize that at the contact surface ($z = 0$ mm) the mole fraction gradients of the species are not necessarily zero due to the differential diffusion of different species and additional thermal diffusion (c.f. Eq.21).

Figure 5: Typical profiles of molle fractions of several species in the flame (gas phase). Combustion system: stoichiometric NH_3-H_2-mixture with 40% hydrogen addition under $p = 1$ bar and $T_{ub} = 300$ K. Flame strain rate: $a = 300$ s^{-1}. Material: Inconel 718.

4.2. Influence of wall materials

In this section, two different wall materials, namely Inconel 718 and Ti-6Al-4V, will be considered and their interaction with the combustion system will be investigated. As a reference, the simulation results considering the material with infinite heat conductivity ($k_s \rightarrow \infty$) will also be presented, which corresponds to the case of no temperature gradient inside the wall ($T(z = 0) = T(-H)$).

Figure 6 first shows the temperature profile in the flame and inside the wall. It is observed that the usage of material with lower heat conductivity (here Ti-6Al-4V) results in a higher contact temperature T_c between the flame and the wall, if the same strain rate imposed in the flame is considered. The higher the heat conductivity of the material is, the lower the contact temperature T_c is. With increasing heat conductivity of the material, the combustion system loses less heat and thus has a higher peak flame temperature.

Based on this observation of the temperature profiles, it is expected that the extinction strain rates (ESR) increase if the heat conductivity of the wall materials also increases. Figure 7 shows the numerically calculated ESR by using Inconel 718, Ti-6Al-4V, and the reference material ($k_s \rightarrow \infty$), namely the ESR against fuel/air equivalence ratios (Φ) for the NH_3-H_2 mixture with 40% H_2 enrichment (upper) and the ESR against hydrogen enrichment (α) for stoichiometric mixture condition.

Firstly, it is observed that the peak extinction limit shifts toward a leaner regime as the wall material has a larger heat conductivity. This can be attributed to the
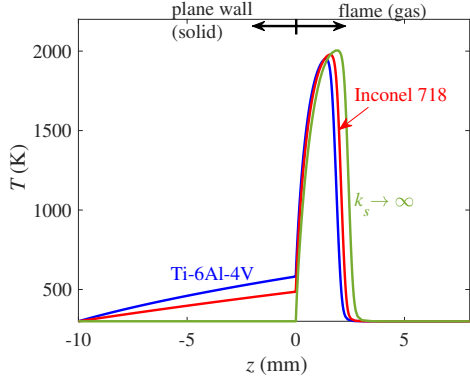
8

Figure 6: Influence of the wall materials on the temperature profile for strain rate a =300 s^{-1}. Combustion system: stoichiometric NH$_3$-H$_2$ mixture with 40% H$_2$ enrichment under $p = 1$ bar and $T_{ub} = 300$ K.

fact that with decreasing heat conductivity of the wall material, the contact temperature becomes higher, leading to increased heat loss. Consequently, more hydrogen in the fuel is required to enhance the chemical reaction. A detailed analysis on this aspect is currently ongoing in our research.

From Fig. 7 it is furthermore observed that due to the larger heat conductivity of Inconel 718, the corresponding flame results in stronger stability against extinction. Although the material made from Inconel 718 is loaded with lower temperature, due to its high Young's modulus and thermal expansion coefficient, it has a much higher maximum of von Mises stresses $\sigma_{vM,max}$ inside the wall for all strain rate cases, as shown in Fig.8. It is observed that the maximum of the $\sigma_{vM,max}$, corresponding to the flame at its extinction limit, of the Inconel 718 could be around two times higher than that of Ti-6Al-4V.

In the following discussion, we will focus on Inconel 718 as the wall material.

4.3. Influence of mixture composition

In this section, the fuel mixture composition will be varied, and the influence on both the flame stability and the mechanical stresses inside the wall will be investigated.

Figure 9 shows the dependence of the extinction strain rates (ESR) on the hydrogen addition α and fuel/air equivalence ratios Φ for unburnt gas mixture with $T_{ub} = 300$ K under $p = 1$ bar and Inconel 718 is used. The increment of Φ in this figure is 0.01. The ESR increases with increasing hydrogen content, and for a certain α the ESR has its maximum at the lean
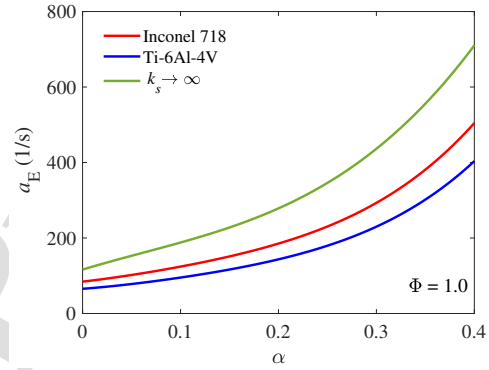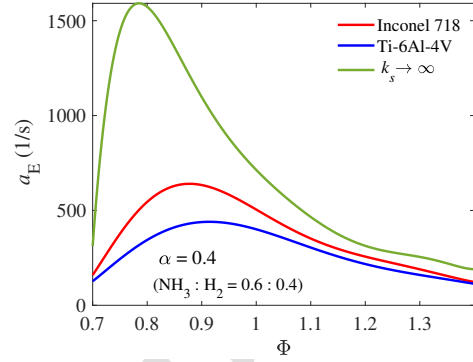

Figure 7: Upper: ESR against fuel/air equivalence ratios (Φ) for the NH$_3$-H$_2$ mixture with 40% H$_2$ enrichment; Lower: ESR against hydrogen enrichment (α) for stoichiometric mixture conditions under $p = 1$ bar and $T_{ub} = 300$ K.

side. With respect to combustion, these results suggest that the flame reaches higher stability against extinction for our considered system if one applies a lean gas mixture with higher hydrogen addition. In the following two sub-sections, the corresponding combustion-induced thermo-mechanical stresses will be discussed.

4.3.1. H$_2$ addition

We begin with the temperature profile in the flame (gas phase) and inside the plane wall (solid phase) for a NH$_3$-H$_2$-air gas mixture with fuel/air equivalence ratio $\Phi = 0.8$ and different levels of hydrogen addition, as shown in Fig.10. The most important observation addressed here is that for the combustion systems imposed with the same strain rate, although greater proportions of hydrogen content α result in higher maximum flame temperature T_{max}, the contact temperature T_c and the temperature distribution inside the plane wall
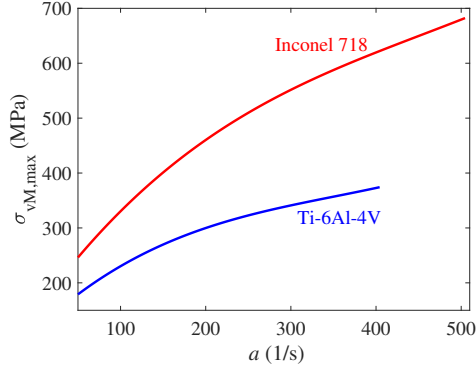
9

Figure 8: Maximum of von Mises stresses $\sigma_{vM,max}$ inside the wall against the flame strain rates for the material use of Inconel 718 and Ti-6Al-4V. Combustion system: stoichiometric NH_3-H_2 mixture with 40% H_2 enrichment under $p = 1$ bar and $T_{ub} = 300$ K.
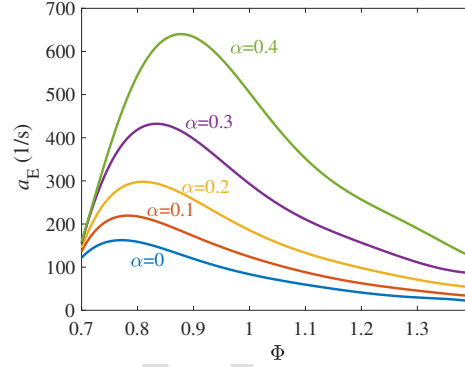

Figure 9: Extinction strain rate a_E over fuel/air equivalence ratios Φ for different levels of hydrogen addition. Combustion system: $T_{ub} = 300$ K, $p = 1$ bar; Material: Inconel 718.

are almost the same. This observation also holds for flames imposed with other strain rates, which is shown in Fig.11(lower) for the T_c against strain rate for gas mixture with different levels of hydrogen addition.

The similarity in contact temperature for different hydrogen contents in the fuel can be attributed to the fact that the heat conductivity of solid material is several orders of magnitude higher than the heat conductivity of gas. Thus, even though the flame temperature increases with increasing hydrogen content α (as confirmed by several other works [71, 72, 73]), the temperature gradient inside the solid is not sensitive to the flame temperature due to its high heat conductivity.

The investigation till now in this sub-section provides the information that if the strain rates are kept unchanged, more hydrogen can be added into the gas mixture to improve the combustion efficiency (e.g. higher flame temperature) without causing higher temperature distribution inside the wall and thus larger thermo-mechanical stresses. However, this does not suggest the use of gas mixture with higher hydrogen content for all cases. In Fig.12 the maximum of von Mises stresses $\sigma_{vM,max}$ inside the wall is plotted against strain rates (till their extinction strain rates) for different hydrogen contents α. We observe that with increasing hydrogen content, although the extinction limit is improved as expected, the possible thermo-mechanical stresses increase also significantly. For example, the NH_3-H_2 with 20% H_2 flame has a maximum of $\sigma_{vM,max}$ of around 520 MPa, while NH_3-H_2 with 40% H_2 flame has a maximum of $\sigma_{vM,max}$ of around 700 MPa. This suggests that the thermo-mechanical stresses become serious as well

with increasing hydrogen content.

4.3.2. Fuel/air equivalence ratio Φ

From Fig.9 it is observed that the extinction strain rates (ESR) change non-monotonically with fuel/air equivalence ratio Φ. In Fig. 13 the maximum of temperature T_{max} of the flame (upper) and the maximum of von Mises stresses $\sigma_{vM,max}$ against strain rates a and fuel/air equivalence ratios Φ are presented for 40%-H_2 addition in fuel, and the increment of Φ is 0.01 (consistent with the one in Fig.9).

It is interesting to observe that for the considered H_2 content in the fuel mixture, the peak extinction strain rate is located in the lean regime, and the peak shifts toward stoichiometry with increasing hydrogen content. As discussed in [63, 74], such phenomenon is attributed to the non-unity Lewis number effects. With increasing H_2 content in fuel (increasing α) and increasing fuel/air equivalence ratio Φ in lean regime, the hydrogen concentration in the reaction zone increases due to differential diffusion effect and the chemical reaction rate is thus enhanced significantly. It is even expected that the peak extinction strain rate shifts further toward fuel-rich regime with continue increase of hydrogen content, as shown in [74] that the peak of laminar flame speed for pure hydrogen/air premixed flame is located at around $\Phi \approx 1.8$.

Consistent with the extinction limit, the flame reaches its highest flame temperature at fuel/air equivalence ratio of around 0.9 for 40%-H_2 addition, and the corresponding combustion-induced maximum of the thermo-mechanical stress (at the extinction limit) also reaches its maxima (c.f. Fig.13). This suggests that the location
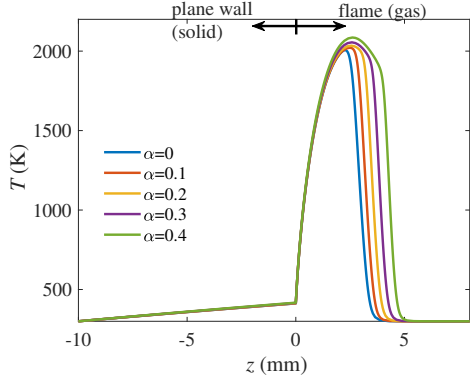
10

Figure 10: Influence of the hydrogen addition α on the temperature profile for strain rate a =100 s^{-1}. Combustion system: NH$_3$-H$_2$ mixture with fuel/air equivalence ratio Φ = 0.8. Combustion system: T_{ub} = 300 K, p = 1 bar; Material: Inconel 718.

of peak flame temperature and peak thermo-mechanical stress are correlated very well with the location of peak extinction limit.

4.4. Influence of combustion pressure

As already shown in many other literatures such as [75, 76, 77], the combustion pressure has a significant effect on the flame structure and chemical reaction, and the flame extinction limit increases with increasing pressure. However, as shown in [59], the increase of pressure also results in an increase of thermo-mechanical stresses in the solid. Therefore, in this section, this observation will be re-visited and the corresponding corrosive behavior at the surface will be discussed due to increased thermal load under high-pressure conditions.

In Fig.14 the temperature profiles inside the plane wall and of the flame are shown for different pressures while keeping all other parameters the same. It is straightforward that with the increase of pressure, the flame becomes narrower and moves closer toward the plane wall (due to slower flame speed). This results in a significant increase in the contact temperature between the flame and the wall surface.

Figure 15 shows at first the effect of pressure on the extinction limits for gas mixture with different hydrogen additions. The tendency shows clearly that the flame becomes more stable against extinction with increasing pressure and hydrogen additions for the considered pressure regime, indicating the advantage of using a high-pressure combustion for the power supply.
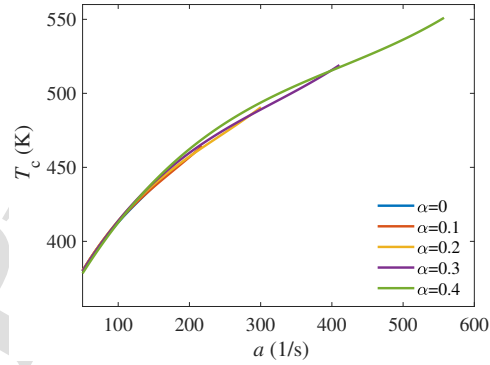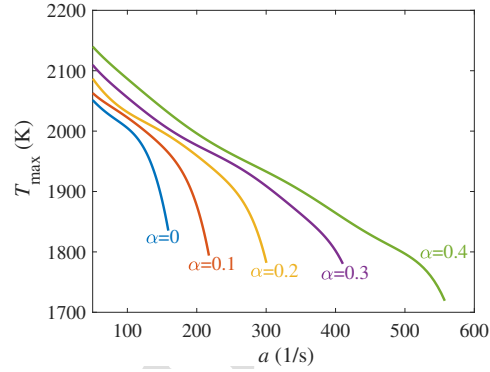

Figure 11: Upper: the ESR against fuel/air equivalence ratios (Φ) for the NH$_3$-H$_2$ mixture with 40% H$_2$ enrichment; Lower: the ESR against hydrogen enrichment (α) for stoichiometric mixture condition. Combustion system: T_{ub} = 300 K, p = 1 bar;

Note that this conclusion will not be altered if the wall is made of other different materials.

However, with the increase of combustion pressure, the contact temperature between the wall and the flame increases as well (c.f. Fig.14). A noticeable high temperature inside the plane wall leads to the fact that the thermo-mechanical stress inside the wall increases significantly as well, as shown in Fig.16. In this figure, the yield strength (red line) is determined according to the temperature profile, which can be obtained from [70]. The von Mises stresses σ_{vM} (black lines) can result in two different behaviors:

- black solid line: this is the regime where $\sigma_{vM} \leq \sigma_Y$, indicating that the plane wall behaves thermo-elastic, and the deformation and induced thermo-mechanical stress disappear after removing the combustion system.
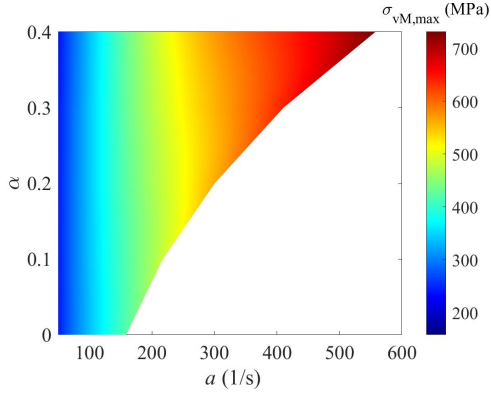
11

Figure 12: Dependence of maximum of von Mises stresses $\sigma_{vM,max}$ inside the wall on strain rate a and hydrogen content α. Combustion system: fuel/air equivalence ratios $\Phi = 0.8$, $T_{ub} = 300$ K, $p = 1$ bar; Material: Inconel 718. White regime: flame extinction regime.

- black dashed line: this is the regime where $\sigma_{vM} > \sigma_Y$. The plane wall would undergo a possible plastic deformation if the loading condition is satisfied, and possible residual stresses exist after removing the flame. In other words, the applied theory of linear thermoelasticity is not valid in this regime and the models including plastic or viscoplastic deformations must be considered.

Since the von Mises stress σ_{vM} inside the wall reaches its possible maximum $\sigma_{vM,max}$ at the contact surface and at the extinction limit, we compare this with the corresponding yield strength σ_Y over the considered pressure ranges in Fig.17. We observe that for a pure ammonia system ($\alpha = 0$) the $\sigma_{vM,max}$ is below the σ_Y for the whole considered pressure. With the increase of hydrogen addition in the gas mixture, the wall is more likely to undergo possible plastic deformation under elevated pressure if the loading condition is satisfied (dashed lines).

4.5. Influence of combustion system on the corrosive behavior

As mentioned above, the parabolic oxidation rate constant k_p (c.f. Sec.2.3), which describes the growth rate of the corrosive layer, depends on the temperature and on the partial pressure of different species. While the values of k_p for Inconel 718 at different temperatures can be found in literature [35], limited oxidation studies were performed for this Ni-based alloy under atmospheric or elevated pressures with different H_2O contents. Moreover, while the parabolic oxidation constant
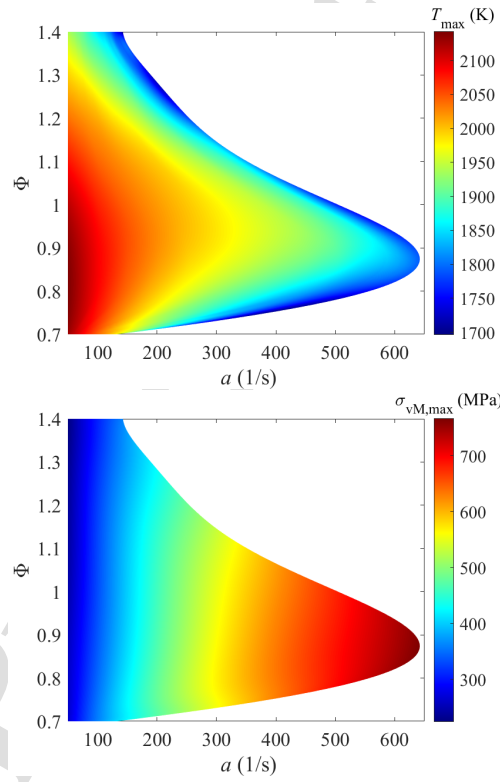

Figure 13: Upper: Dependence of maximum of temperature T_{max} of the flame on strain rate a and fuel/air equivalence ratios Φ; Lower: Dependence of maximum of von Mises stresses $\sigma_{vM,max}$ inside the wall on strain rate a and fuel/air equivalence ratios Φ. Combustion system: hydrogen content $\alpha = 0.4$, $T_{ub} = 300$ K, $p = 1$ bar; Material: Inconel 718. White regime: flame extinction regime.

k_p decreased significantly with decreasing O2 partial pressure generally [78], the studies showing the dependence of parabolic oxidation constant on the water partial pressure revealed contradictory results. Young [32] claims that the oxidation kinetics accelerates with increasing H2O, while Simon et al. [79] observed that the k_p values of a binary alloy Ni-25Cr (the chemical composition is similar to that of Inconel 718) decreases with enhancing H_2O content at a constant $p(O_2)$ [79]. Therefore, in this section we focus on the relation between water partial pressure $p(H_2O)$ or oxygen partial pressure $p(O_2)$ at the stagnation point $z = 0$ and contact temperature T_c, which is shown in Fig.18 where the combustion pressure is set to be $p = 1$ bar.

From this figure, it is interesting to see that the water partial pressure is less dependent on the hydrogen
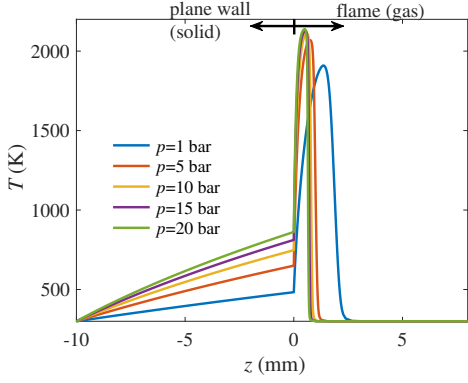
12

Figure 14: Influence of pressure on the temperature profile for strain rate a = 300 s^{-1}. Combustion system: hydrogen addition α = 0.4, fuel/air equivalence ratios Φ = 1.1, T_{ub} = 300 K; Material: Inconel 718.
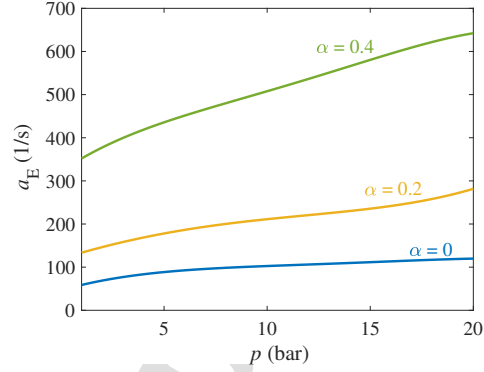

Figure 15: Influence of pressure on the extinction limits for different hydrogen addition. Combustion system: fuel/air equivalence ratios Φ = 1.1, T_{ub} = 300 K; Material: Inconel 718.

addition in gas mixture but is a strong function of the equivalence ratio. The reason can be considered as follows:

- with the increase in hydrogen content in the gas mixture, we obtain the mole fraction of hydrogen in the fuel mixture according to Eq.24 as:

$$x(\text{H-element}) = \frac{3 - \alpha}{17 - 15\alpha}. \quad (25)$$

This suggests a mild increase in the hydrogen element within the hydrogen addition range of 0% to 40%, with the increase ranging from 0.1765 to 0.2364. Therefore, despite different hydrogen additions, the total amount of hydrogen element does not change significantly. Consequently, the H$_2$O concentration and, consequently, the water partial pressure do not change significantly with different hydrogen content.

- However, if the fuel/air equivalence ratio changes, the hydrogen element in the total mixture (fuel + air) changes significantly. Consequently, the amount of hydrogen required to produce H$_2$O can vary considerably.

Note that the dependence of H$_2$O concentration in the product on fuel/air equivalence ratios, rather than on the hydrogen addition in fuel, has also been confirmed through experimental measurements [80].

Related to the corrosion behaviors, two main conclusions can be drawn:

- As discussed above, the contact temperature T_c between the plane wall and the flame increases with increasing flame strain rate. Therefore, if the flame is imposed with higher strain rate, the T_c also becomes larger, which would accelerate the corrosive layer growth (c.f. Eq.19). However, the increase of T_c results in an increase of water vapor partial pressure $p(\text{H}_2\text{O})$ and oxygen partial pressure $p(\text{O}_2)$ as well for a certain gas mixture. The dependence of corrosive parabolic rate constant on both partial pressures for the Inconel 718 is still unknown, which requires more study in the future.

- Since water vapor is the main product in the exhaust gas while the oxygen is consumed to a large amount during the combustion reaction, leading to the fact that $p(\text{O}_2) \ll p(\text{H}_2\text{O})$ (in this example around three order of magnitude lower). As reported in [78], the parabolic oxidation constant decreases significantly to a very low level if the oxygen partial pressure $p(\text{O}_2)$ is below 0.1 MPa. Hence, it is believed that under the combustion condition, the water vapor plays more important role on the formation of oxide layer than the oxygen.

- Keeping the fuel/air equivalence ratios, the relation between $p(\text{H}_2\text{O})$ and T_c remains similar for gas mixtures with different hydrogen contents, suggesting a similar corrosive parabolic rate constant k_p.

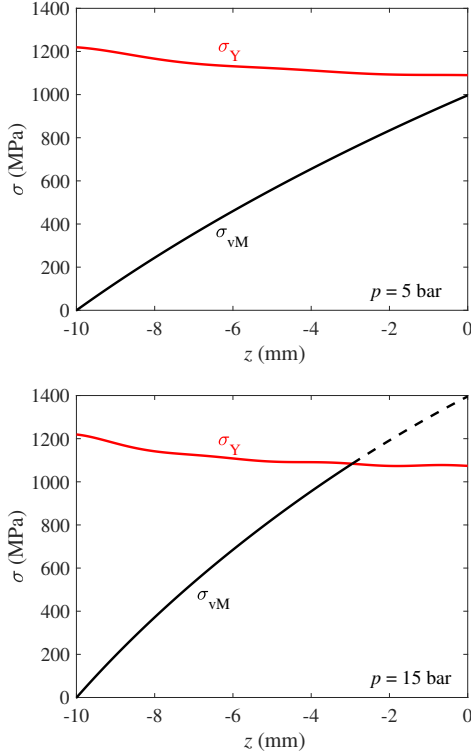- Since the $p(\text{H}_2\text{O})$ depends significantly on the fuel/air equivalence ratio Φ, the impact of Φ on

13

Figure 16: Comparison of σ_{vM} and σ_Y for flame with strain rate $a = 300$ s^{-1} for two different pressures. Combustion system: hydrogen addition $\alpha = 0.4$, fuel/air equivalence ratios $\Phi = 1.1$, $T_{ub} = 300$ K; Material: Inconel 718.

the consequent change of corrosive parabolic rate constant k_p is expected to be noticeable as well, requiring more investigation.

4.6. Influence of surface reaction

All the results presented above involve numerical simulations without considering surface reactions at the wall surface. In this section, we will briefly examine the potential impact of surface reactions on the combustion system. We adopt the simple surface reaction model described in [51], which includes five recombination/destruction reactions of reactive molecules on the
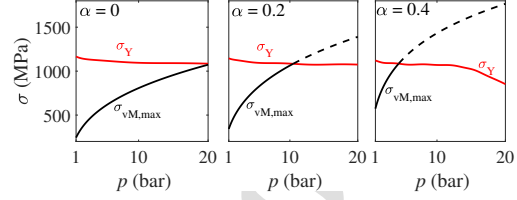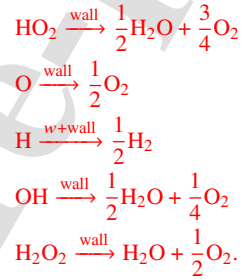

Figure 17: The possible maximum of the von Mises stress σ_{vM} inside the wall (at the contact surface and at the extinction limit) for gas mixtures with three different hydrogen additions. Combustion system: fuel/air equivalence ratios $\Phi = 1.1$, $T_{ub} = 300$ K; Material: Inconel 718.

surface, as follows:

$$HO_2 \xrightarrow{wall} \frac{1}{2}H_2O + \frac{3}{4}O_2$$

$$O \xrightarrow{wall} \frac{1}{2}O_2$$

$$H \xrightarrow{w+wall} \frac{1}{2}H_2$$

$$OH \xrightarrow{wall} \frac{1}{2}H_2O + \frac{1}{4}O_2$$

$$H_2O_2 \xrightarrow{wall} H_2O + \frac{1}{2}O_2.$$

Note that here the NH$_3$ decomposition reactions at the surface are not included for simplification. The aim at this stage is only to gain some information to what extent the surface reactions are important. After including these simple surface reactions in the numerical simulation, spatial profiles of temperature and mole fractions of different species are compared in Fig.19, where the NH$_3$-H$_2$ mixture with 40% H$_2$ enrichment is used and strain rate $a = 200$s^{-1} is imposed in the flame.

From the temperature profile, it is observed that including surface reactions in this case has a minor effect on the temperature. The contact temperature decreases by only around 20 K, which is expected to result in a minor change in thermal-mechanical stress.

From the species profiles, it is observed that the concentration of H radical is affected to some extent by the surface reactions in most regimes. The water mole fraction, on the other hand, changes noticeably near the surface regime when the surface reaction is considered. Since the water partial pressure is an important indicator for predicting the parabolic oxidation rate at the wall surface, this result suggests that including the surface reaction could provide a more accurate prediction for the formation of the oxide layer.

As a part of ongoing research, a more detailed model for surface reactions, including absorption and desorp-
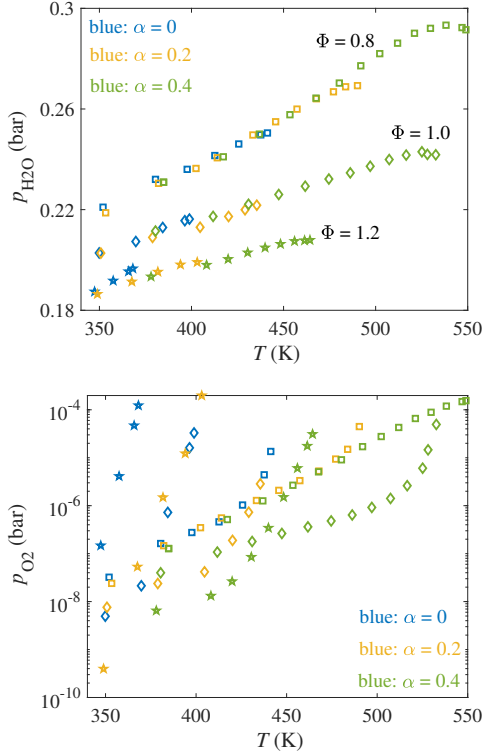
14

Figure 18: Dependence of water partial pressure $p(H_2O)$ (upper) and oxygen partial pressure $p(H_2O)$ (lower) on contact temperature T_c for different fuel/air equivalence ratios Φ and hydrogen contents α. Combustion system: $p = 1$ bar. Material: Inconel 718. ■: $\Phi = 0.8$; ◆: $\Phi = 1.0$; ★: $\Phi = 1.2$.

tion, will be considered to predict the radicals adhered to the surface.

5. Conclusions

In the present work, the steady stagnation flow flame to a plane wall is numerically investigated with a focus on the flame extinction limit and its influence on the wall materials. The thermo-mechanical stress and the corrosive behavior inside and at the surface of the plane wall are considered indicators, if the solid interacts with the flame. The NH_3-H_2-air gas mixture is selected as a zero-carbon fuel that can be used for practical next-generation systems for energy transportation, storage, and power generation. The major conclusions from this work are:

- the extinction limits become larger, if the wall material with higher heat conductivity is used.

- an increase in hydrogen addition in the NH_3-H_2 gas fuel improves the combustion efficiency such as higher flame temperature and higher extinction limit. Furthermore, the thermo-mechanical stresses stay at a similar level if the flame is imposed with the same strain rate. However, the solid wall can be loaded with higher thermo-mechanical stresses, if the combustion system is burnt with a gas mixture with higher hydrogen addition.

- for H_2 content less than 40%-vol in the fuel, the flame exhibits its highest extinction limit in the lean regime, and the location of the peak extinction limit shifts toward an increasing fuel/air equivalence ratio with an increase in hydrogen content. However, it is noteworthy that the location of the peak extinction limit corresponds to the location of the combustion-induced maximum thermo-mechanical stress inside the wall.

- flame becomes more stable against extinction at high pressures. Meanwhile, the material is more likely to undergo a plastic deformation under high combustion pressure with higher hydrogen addition, if the corresponding loading condition is satisfied.

- the effect of combustion system on the corrosive behavior in terms of corrosive parabolic rate constant is not straightforward, since the partial pressures of water vapor vary significantly and there are limited results from the literature. However, qualitatively speaking, the corrosive parabolic rate constant remains similar for gas mixtures with different hydrogen contents at the same fuel/air equivalence ratios.

As ongoing research, the plasticity will be modeled, which renders the mechanical problem physically nonlinear. And the corrosive parabolic rate constants under the conditions related to the combustion processes will also be experimental investigated.

15
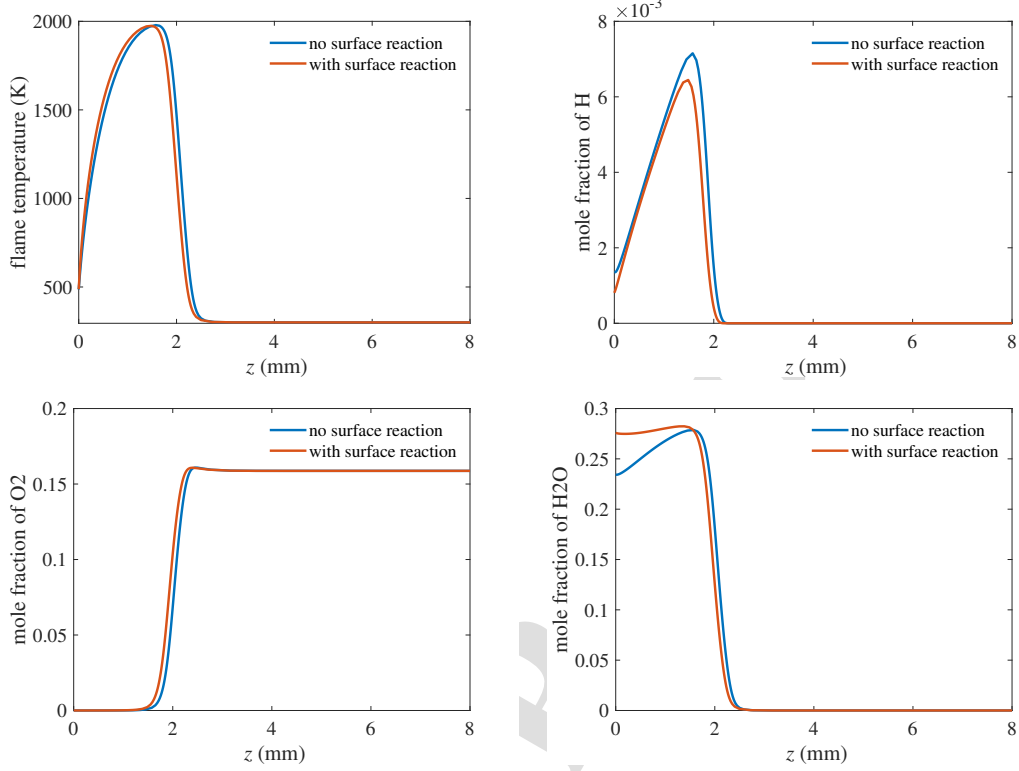
Figure 19: Spatial profiles of temperature and mole fractions of different species with and without surface reaction for the NH_3-H_2 mixture with 40% H_2 enrichment and strain rate $a = 200s^{-1}$. Combustion system: T_{ub} = 300 K, p = 1 bar

Appendix A. Material Properties

Thermo-physical properties of Inconel-718 are outlined, which are all functions of temperature.

- heat conductivity k in W/(m · K):

$$k(T) = 7.69 + 0.0146 \cdot \frac{T}{K}. \quad (A.1)$$

- thermal expansion coefficient α in 1/K [81]:

$$\alpha(T) = 1.069 \times 10^{-5} + 1.233 \times 10^{-9} \cdot \frac{T}{K}. \quad (A.2)$$

- Poisson's ratio ν [82]:

$$\nu(T) = 0.28. \quad (A.3)$$

- Young's modulus E in GPa [83]:

$$E(T) = 228.6 - 0.13 \cdot \frac{T}{K} + 1.47 \times 10^{-4} \cdot \left(\frac{T}{K}\right)^2$$
$$- 8.834 \times 10^{-8} \cdot \left(\frac{T}{K}\right)^3. \quad (A.4)$$

Thermo-physical properties of the Ti-6Al-4V material are outlined according to Tanigawa et.al. [84], which are all functions of temperature:

- heat conductivity k in W/(m · K):

$$k(T) = 1.1 + 0.017 \cdot \frac{T}{K}. \quad (A.5)$$

- thermal expansion coefficient α in 1/K:

$$\alpha(T) = \begin{cases} 7.43 \times 10^{-6} + 5.56 \times 10^{-9} \cdot \frac{T}{K} - 2.9 \times 10^{-12} \cdot \left(\frac{T}{K}\right)^2, \\ (300K \leq T \leq 1100K) \\ 10.291 \times 10^{-6}, \\ (1100K \leq T \leq 1300K) \end{cases}$$
$$(A.6)$$

- Poisson's ratio ν:

$$\nu(T) = 0.2888 + 32.0 \times 10^{-6} \cdot \frac{T}{K}. \quad (A.7)$$

- Young's modulus E in GPa:

$$E(T) = 122.7 - 0.0565 \cdot \frac{T}{K}. \quad (A.8)$$

16

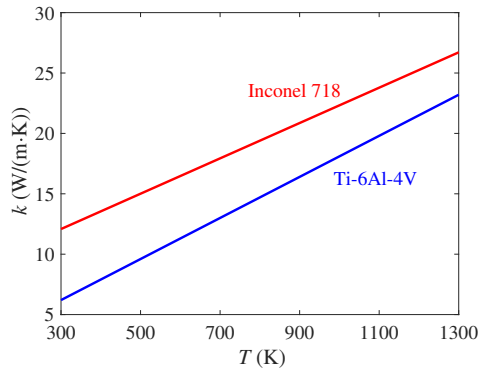Figures A.20 - A.23 represent the comparison of each material properties between the Inconel 718 and the Ti-6Al-4V.

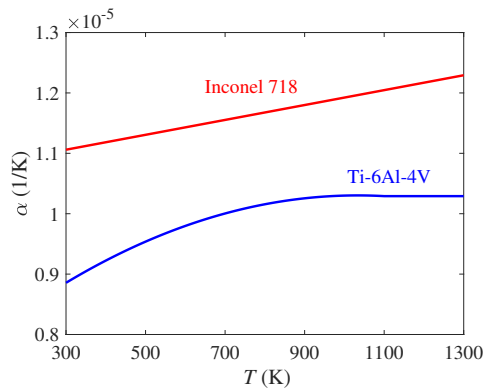Figure A.20: Temperature-dependent heat conductivity.

Figure A.21: Temperature-dependent thermal expansion coefficient.

Figure A.22: Temperature-dependent Poisson's ratio.

Figure A.23: Temperature-dependent Young's modulus.

References

[1] T. Á. Tejedor, Gas turbine materials selection, life management and performance improvement, Power Plant Life Management and Performance Improvement (2011) 330–419.

[2] K. Mukai, H. Miyazaki, The influence of the combustion chamber head material of a gasoline engine on exhaust hc, SAE transactions (2000) 2119–2126.

[3] E. Benini, Advances in gas turbine technology, BoD–Books on Demand, 2011.

[4] H. Moon, K. M. Kim, Y. H. Jeon, S. Shin, J. S. Park, H. H. Cho, Effect of thermal stress on creep lifetime for a gas turbine combustion liner, Engineering Failure Analysis 47 (2015) 34–40.

[5] Y. Xia, P. Sharkey, I. Verma, A. Khaware, D. Cokljat, Prediction of thermoacoustic instability and fluid–structure interactions for gas turbine combustor, Journal of Engineering for Gas Turbines and Power 144 (9) (2022) 091005.

[6] A. Valera-Medina, H. Xiao, M. Owen-Jones, W. I. David, P. Bowen, Ammonia for power, Progress in Energy and combustion science 69 (2018) 63–102.

[7] A. Valera-Medina, F. Amer-Hatem, A. Azad, I. Dedoussi, M. De Joannon, R. Fernandes, P. Glarborg, H. Hashemi, X. He, S. Mashruk, et al., Review on ammonia as a potential fuel: from synthesis to economics, Energy & Fuels 35 (9) (2021) 6964–7029.

[8] N. Zhang, R. Komoda, K. Yamada, M. Kubota, A. Staykov, Ammonia mitigation and induction effects on hydrogen environment embrittlement of scm440 low-alloy steel, International Journal of Hydrogen Energy 47 (33) (2022) 15084–15093.

[9] M. Kovaleva, D. Dziedzic, S. Mashruk, S. Evans, A. Valera-Medina, E. Galindo-Nava, The evaluation of ammonia/hydrogen combustion on the h permeation and embrittlement of nickel-base superalloys, in: Turbo Expo: Power for Land, Sea, and Air, Vol. 86052, American Society of Mechanical Engineers, 2022, p. V007T17A011.
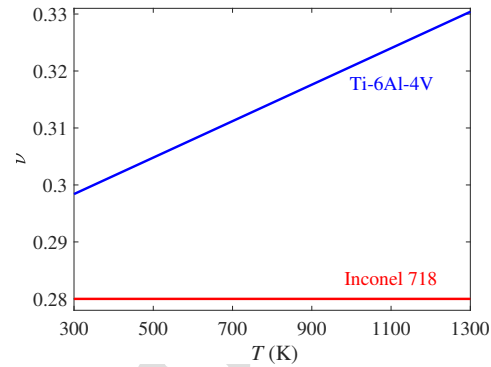
[10] M. Kutz, Handbook of environmental degradation of materials, William Andrew, 2018.

[11] E. E. Stansbury, R. A. Buchanan, Fundamentals of electrochemical corrosion, ASM international, 2000.

[12] N. Bouvet, D. Davidenko, C. Chauveau, L. Pillier, Y. Yoon, On the simulation of laminar strained flames in stagnation flows: 1d and 2d approaches versus experiments, Combustion and flame 161 (2) (2014) 438–452.

[13] J. M. Bergthorson, S. D. Salusbury, P. E. Dimotakis, Experiments and modelling of premixed laminar stagnation flame hydrodynamics, Journal of fluid mechanics 681 (2011) 340–369.

[14] A. Hayakawa, Y. Hirano, E. C. Okafor, H. Yamashita, T. Kudo, H. Kobayashi, Experimental and numerical study of product gas characteristics of ammonia/air premixed laminar flames stabilized in a stagnation flow, Proceedings of the Combustion Institute 38 (2) (2021) 2409–2417.

[15] F. N. Egolfopoulos, H. Zhang, Z. Zhang, Wall effects on the propagation and extinction of steady, strained, laminar premixed flames, Combustion and Flame 109 (1-2) (1997) 237–252.

[16] G. Stahl, J. Warnatz, Numerical investigation of time-dependent properties and extinction of strained methane- and propane-air flamelets, Combustion and flame 85 (3-4) (1991) 285–299.

[17] R. J. Kee, J. A. Miller, G. H. Evans, G. Dixon-Lewis, A computational model of the structure and extinction of strained, opposed flow, premixed methane-air flames, in: Symposium (International) on Combustion, Vol. 22, Elsevier, 1989, pp. 1479–1494.

[18] J. Warnatz, U. Maas, R. W. Dibble, J. Warnatz, Combustion, Springer, Berlin, Heidelberg, 2006.

[19] J. O. Hirschfelder, C. F. Curtiss, R. B. Bird, M. G. Mayer, Molecular theory of gases and liquids, Vol. 165, Wiley New York, 1964.

[20] H. Bongers, L. De Goey, The effect of simplified transport modeling on the burning velocity of laminar premixed flames, Combustion science and technology 175 (10) (2003) 1915–1928.

[21] G. Ribert, N. Zong, V. Yang, L. Pons, N. Darabiha, S. Candel, Counterflow diffusion flames of general fluids: Oxygen/hydrogen mixtures, Combustion and Flame 154 (3) (2008) 319–330.

[22] I. M. Daniel, O. Ishai, I. M. Daniel, I. Daniel, Engineering mechanics of composite materials, Vol. 1994, Oxford university press New York, 2006.

[23] A.-R. A. Ragab, S. E. A. Bayoumi, Engineering solid mechanics: fundamentals and applications, Routledge, 2018.

[24] M. R. Eslami, R. B. Hetnarski, J. Ignaczak, N. Noda, N. Sumi, Y. Tanigawa, Theory of elasticity and thermal stresses, Vol. 197, Springer, Dordrecht, 2013.

[25] M. E. Gurtin, An introduction to continuum mechanics, Academic press, New York, 1982.

[26] F. Dunne, N. Petrinic, Introduction to computational plasticity, OUP Oxford, 2005.

[27] R. B. Bird, W. E. Stewart, E. N. Lightfoot, Transport phenomena, Wiley New York, 2006.

[28] B. Schweizer, J. Wauer, Atomistic explanation of the gough-joule-effect, The European Physical Journal B-Condensed Matter and Complex Systems 23 (2001) 383–390.

[29] A. P. Boresi, R. J. Schmidt, O. M. Sidebottom, et al., Advanced mechanics of materials, Vol. 6, Wiley New York, 1985.

[30] G. Boothroyd, C. Poli, Applied Engineering Mechanics: Statics and Dynamics, Routledge, 2018.

[31] D. Gross, W. Ehlers, P. Wriggers, J. Schröder, R. Müller, Mechanics of Materials-Formulas and Problems, Springer Berlin, Heidelberg, 2016.

[32] D. J. Young, High temperature oxidation and corrosion of metals, Vol. 1, Elsevier, 2008.

[33] C. Ahner, P. Maaß, P. Peißker, Handbook of hot-dip galvanization, John Wiley & Sons, 2011.

[34] G. Frankel, Fundamentals of corrosion kinetics, Active protective coatings: new-generation coatings for metals (2016) 17–32.

[35] I. G. Wright, R. Dooley, A review of the oxidation behaviour of structural alloys in steam, International Materials Reviews 55 (3) (2010) 129–167.

[36] S. Saunders, M. Monteiro, F. Rizzo, The oxidation behaviour of metals and alloys at high temperatures in atmospheres containing water vapour: A review, Progress in materials science 53 (5) (2008) 775–837.

[37] N. Birks, G. H. Meier, F. S. Pettit, Introduction to the high temperature oxidation of metals, Cambridge university press, 2006.

[38] M. A. Imam, J. S. Young, R. G. Reddy, Effect of oxygen partial pressure and temperature on the oxidation behavior of SiB6, Metallurgical and Materials Transactions B 51 (1) (2020) 386–394.

[39] H. Sakai, T. Tsuji, K. Naito, Effect of oxygen partial pressure on oxidation of iron at 573 k, Journal of Nuclear Science and Technology 21 (11) (1984) 844–852.

[40] M. de Fátima Salgado, I. S. Carvalho, R. S. Santos, J. A. S. Porto, O. V. Correa, L. V. Ramanathan, A. de Sá Brandim, V. F. Lins, Effect of oxygen partial pressure on oxidation behavior of ferritic stainless steel aisi 441 at high temperatures, Engineering Failure Analysis 105 (2019) 215–226.

[41] E. J. Opila, R. E. Hann Jr, Paralinear oxidation of cvd sic in water vapor, Journal of the American Ceramic Society 80 (1) (1997) 197–205.

[42] L. F. Santos, J. A. Moreno, J. Orozco-Agamez, V. V. Kafarov, A. Y. Leon, D. Peña, Effects of temperature and pressure on corrosion products in a steam-flue gas envirorment: A simulation study, Chemical Engineering Transactions 94 (2022) 253–258.

[43] J. Wanklyn, C. Britton, D. Silvester, N. Wilkins, Influence of environment on the corrosion of zirconium and its alloys in high-temperature steam, Journal of the Electrochemical Society 110 (8) (1963) 856.

[44] Y. Jacob, V. Haanappel, M. F. Stroosnijder, H. Buscail, P. Fielitz, G. Borchardt, The effect of gas composition on the isothermal oxidation behaviour of pm chromium, Corrosion Science 44 (9) (2002) 2027–2039.

[45] C. Anghel, E. Hörnlund, G. Hultquist, M. Limbäck, Gas phase analysis of co interactions with solid surfaces at high temperatures, Applied Surface Science 233 (1-4) (2004) 392–401.

[46] P. Feng, M. Lee, D. Wang, Y. Suzuki, Ammonia thermal decomposition on quartz and stainless steel walls, International Journal of Hydrogen Energy (2023).

[47] S. Appari, V. M. Janardhanan, S. Jayanti, L. Maier, S. Tischer, O. Deutschmann, Micro-kinetic modeling of nh3 decomposition on ni and its application to solid oxide fuel cells, Chemical engineering science 66 (21) (2011) 5184–5191.

[48] P. Aghalayam, P. Bui, D. Vlachos, The role of radical wall quenching in flame stability and wall heat flux: hydrogen-air mixtures, Combustion Theory and Modelling 2 (4) (1998) 515.

[49] K. T. Kim, D. H. Lee, S. Kwon, Effects of thermal and chemical surface–flame interaction on flame quenching, Combustion and flame 146 (1-2) (2006) 19–28.

[50] Y. Fan, J. Guo, M. Lee, N. Iki, Y. Suzuki, Quantitative evaluation of wall chemical effect in hydrogen flame using two-photon absorption lif, Proceedings of the Combustion Institute 38 (2) (2021) 2361–2370.

[51] U. Maas, J. Warnatz, Ignition processes in hydrogen- oxygen mixtures, Combustion and flame 74 (1) (1988) 53–69.

[52] İ. B. Özdemir, N. Lippmann, Modeling and simulation of surface reactions and reactive flow of a nitriding process, Surface and Coatings Technology 219 (2013) 151–162.

18

[53] D. Wang, M. Lee, Y. Suzuki, Nitriding effects of ammonia flames on iron-based metal walls, Journal of Ammonia Energy 1 (1) (2023).

[54] L. Garcia-Fresnillo, A. Chyrkin, C. Böhme, J. Barnikel, F. Schmitz, W. J. Quadakkers, Oxidation behaviour and microstructural stability of alloy 625 during long-term exposure in steam, Journal of materials science 49 (2014) 6127–6142.

[55] C. Yu, S. Eckart, S. Essmann, D. Markus, A. Valera-Medina, R. Schießl, B. Shu, H. Krause, U. Maas, Investigation of spark ignition processes of laminar strained premixed stoichiometric nh3-h2-air flames, Journal of Loss Prevention in the Process Industries 83 (2023) 105043.

[56] D. Markus, H.-P. Schildberg, W. Wildner, G. Krdzalic, U. Maas, Flammability limits of premixed methane/methanol/air flames, Combustion Science and Technology 175 (11) (2003) 2095–2112.

[57] S. Eckart, C. Yu, U. Maas, H. Krause, Experimental and numerical investigations on extinction strain rates in non-premixed counterflow methane and propane flames in an oxygen reduced environment, Fuel 298 (2021) 120781.

[58] C. Strassacker, V. Bykov, U. Maas, Redim reduced modeling of quenching at a cold wall including heterogeneous wall reactions, International Journal of Heat and Fluid Flow 69 (2018) 185–193.

[59] C. Yu, T. Boehlke, A. Valera-Medina, B. Yang, U. Maas, Flame–solid interaction: Thermomechanical analysis for a steady laminar stagnation flow stoichiometric nh3–h2 flame at a plane wall, Energy & Fuels 37 (4) (2023) 3294–3306.

[60] P. P. Walsh, P. Fletcher, Gas turbine performance, Wiley New Jersey, 2004.

[61] M. P. Boyce, Gas turbine engineering handbook, Elsevier, 2011.

[62] R. Li, A. A. Konnov, G. He, F. Qin, D. Zhang, Chemical mechanism development and reduction for combustion of nh3/h2/ch4 mixtures, Fuel 257 (2019) 116059.

[63] M. Richter, R. Schultheis, J. Dawson, A. Gruber, R. Barlow, A. Dreizler, D. Geyer, Extinction strain rates of premixed ammonia/hydrogen/nitrogen-air counterflow flames, Proceedings of the Combustion Institute 39 (2) (2023) 2027–2035.

[64] M. Boivineau, C. Cagran, D. Doytier, V. Eyraud, M.-H. Nadal, B. Wilthan, G. Pottlacher, Thermophysical properties of solid and liquid ti-6al-4v (ta6v) alloy, International journal of thermophysics 27 (2) (2006) 507–529.

[65] M. Niinomi, Mechanical properties of biomedical titanium alloys, Materials Science and Engineering: A 243 (1-2) (1998) 231–236.

[66] E. Hosseini, V. Popovich, A review of mechanical properties of additively manufactured inconel 718, Additive Manufacturing 30 (2019) 100877.

[67] S. Liu, Y. C. Shin, Additive manufacturing of ti6al4v alloy: A review, Materials & Design 164 (2019) 107552.

[68] D. Deng, Additively Manufactured Inconel 718: Microstructures and Mechanical Properties, Vol. 1798, Linköping University Electronic Press, 2018.

[69] F. Wang, S. Williams, P. Colegrove, A. A. Antonysamy, Microstructure and mechanical properties of wire and arc additive manufactured ti-6al-4v, Metallurgical and Materials Transactions A 44 (2013) 968–977.

[70] Y. Zhang, T. T. Zuo, Z. Tang, M. C. Gao, K. A. Dahmen, P. K. Liaw, Z. P. Lu, Microstructures and properties of high-entropy alloys, Progress in materials science 61 (2014) 1–93.

[71] T. B. Imhoff, S. Gkantonas, E. Mastorakos, Analysing the performance of ammonia powertrains in the marine environment, Energies 14 (21) (2021) 7447.

[72] A. Valera-Medina, D. Pugh, P. Marsh, G. Bulat, P. Bowen, Preliminary study on lean premixed combustion of ammonia-hydrogen for swirling gas turbine combustors, International Journal of Hydrogen Energy 42 (38) (2017) 24495–24503.

[73] J. Otomo, M. Koshi, T. Mitsumori, H. Iwasaki, K. Yamada, Chemical kinetic modeling of ammonia oxidation with improved reaction mechanism for ammonia/air and ammonia/hydrogen/air combustion, International Journal of Hydrogen Energy 43 (5) (2018) 3004–3014.

[74] A. L. Sánchez, F. A. Williams, Recent advances in understanding of flammability characteristics of hydrogen, Progress in Energy and Combustion Science 41 (2014) 1–55.

[75] C. Sohn, I. Jeong, S. Chung, Numerical study of the effects of pressure and air-dilution on no formation in laminar counterflow diffusion flames of methane in high temperature air, Combustion and Flame 130 (1-2) (2002) 83–93.

[76] U. Niemann, K. Seshadri, F. A. Williams, Methane, ethane, and ethylene laminar counterflow diffusion flames at elevated pressures: Experimental and computational investigations up to 2.0 mpa, Combustion and Flame 161 (1) (2014) 138–146.

[77] S. Colson, A. Hayakawa, T. Kudo, H. Kobayashi, Extinction characteristics of ammonia/air counterflow premixed flames at various pressures, Journal of Thermal Science and Technology 11 (3) (2016) JTST0048–JTST0048.

[78] Z. Yu, D. Zeng, Y. Lin, G. Zeng, Y. Feng, B. Ding, H. Li, Investigations on the oxygen corrosion behaviors of p110 steel in a dynamic experiment simulating nitrogen injection, Materials and Corrosion 71 (8) (2020) 1375–1385.

[79] D. Simon, B. Gorr, H. J. Christ, Effect of atmosphere and sample thickness on kinetics, microstructure, and compressive stresses of chromia scale grown on ni–25cr, Oxidation of Metals 87 (2017) 417–429.

[80] C. Yu, Z. Chen, U. Maas, A. Valera-Medina, b. Yang, Assessment of thermal radiation effect on ammonia-hydrogen-air laminar unstrained premixed flames at atmospheric and elevated pressures, submitted, under review.

[81] K. K. AM, P. Kuppusami, T. Dharini, Thermal expansion studies of electron beam evaporated yttria films on inconel-718 substrates, Surface and Coatings Technology 354 (2018) 297–305.

[82] S. Subramanian, A. Sekhar, B. Prasad, Influence of combined radial location and growth on the leakage performance of a rotating labyrinth gas turbine seal, Journal of Mechanical Science and Technology 29 (2015) 2535–2545.

[83] S. Seo, O. Min, H. Yang, Constitutive equation for ti–6al–4v at high temperatures measured using the shpb technique, International journal of impact engineering 31 (6) (2005) 735–754.

[84] Y. Tanigawa, T. Akai, R. Kawamura, N. Oka, Transient heat conduction and thermal stress problems of a nonhomogeneous plate with temperature-dependent material properties, Journal of Thermal Stresses 19 (1) (1996) 77–102.

19

Highlights of the paper

- The steady laminar stagnation flow ammonia/hydrogen/air flame to a plane wall is numerical investigated.
- The effect of wall material on the flame stability against extinction is discussed.
- The effect of combustion process on the thermo-mechanical stress in the wall material is investigated.
- The effect of combustion process on the corrosive behavior at the wall surface is studied.

Declaration of interests

☒ The authors declare that they have no known competing financial interests or personal relationships that could have appeared to influence the work reported in this paper.

☐The authors declare the following financial interests/personal relationships which may be considered as potential competing interests: